Electronic Supplementary Material (ESI) for Physical Chemistry Chemical Physics.

Support Information: The Role of the Coordination Effect in Single Atom Rh Dopant on Ag(211) for OH and CO Adsorption

Marionir M. C. B. Neto,*,† Lucas G. Verga ,*,‡ Juarez L. F. Da Silva,*,‡ and Breno R. L. Galvão*,†

†*Centro Federal de Educação Tecnológica de Minas Gerais, CEFET-MG, Av. Amazonas 5253, (30421-169) Belo Horizonte, Minas Gerais, Brazil*

‡*São Carlos Institute of Chemistry, University of São Paulo, P.O. Box 780, 13560-970, São Carlos, SP, Brazil*

E-mail: marioniir@hotmail.com; lucas.gverga@usp.br; juarez_dasilva@iqsc.usp.br; brenogalvao@gmail.com

Contents

1 Computational Parameters **S-2**

2 Effective Coordination Concept **S-3**

3 Gas-phase Molecules **S-3**

4 Bulk Ag Properties **S-4**

5 Stepped Ag(211) Clean Surface **S-6**

6 Substitution Doping Rh@Ag(211) S-9

7 Adsorption Properties S-11

7.1 Adsorption Sites S-11

7.2 Adsorption of OH on Ag(211) S-12

7.3 Adsorption of CO on Ag(211) S-12

7.4 Adsorption of OH on Rh@Ag(211) S-13

7.5 Adsorption of CO on Rh@Ag(211) S-13

7.6 Gibbs Free Energies of Adsorption S-14

7.7 Adsorption Barrier S-15

7.8 Adsorption on nanoclusters and benchmarking S-17

References S-19

1 Computational Parameters

All calculations performed in this work were carried out with the Vienna *Ab initio* Simulation Package (VASP). Table S1 shows the details related to the Projector Augmented Wave (PAW) projectors used as `POTCAR` files.[1,2]

Table S1 Relevant parameters of the PAW projectors. For each element, we show the chosen projector, the number of valence electrons (`ZVAL`), the electronic configuration and the recommended plane-wave cutoff energy (`ENMAX`) given in the `POTCAR` file.

Element	PAW-PBE Projectors	`ENMAX` (eV)	Eletronic Configuration	`ZVAL`
Ag	Ag_GW 06Mar2008	249.844	[Kr] $4d^{10}5s^1$	11
C	C_GWnew 19Mar2012	413.992	[He] $2s^2 2p^2$	4
O	O_GWnew 19Mar2012	434.431	[He] $2s^2 2p^4$	6
H	H_GW 21Apr2008	300.000	$1s^1$	1
Rh	Rh_GW 06Mar2008	247.408	[Kr] $4d^8 5s^1$	9

2 Effective Coordination Concept

The coordination number (CN) is an useful concept to rationalize the properties of different sites on a surface. This quantity is simply expressed as the number of nearest neighbors of a given atom i and assumes an integer value. This concept can be improved by giving different weights for each neighbor based on the distance between atoms (d_{ij}). In this work we use the Effective Coordination Number (ECN) concept,[3,4] and within this approach one first defines an average bond length for atom i as

$$d_{av}^{i} = \frac{\sum_j d_{ij} \exp\left[1 - \left(\frac{d_{ij}}{d_{av}^{i}}\right)^6\right]}{\sum_j \exp\left[1 - \left(\frac{d_{ij}}{d_{av}^{i}}\right)^6\right]}, \tag{1}$$

which is obtained self-consistently. The effective coordination number of atom i (ECN_i) is then obtained as

$$\mathrm{ECN}_i = \sum_j \exp\left[1 - \left(\frac{d_{ij}}{d_{av}^{i}}\right)^6\right]. \tag{2}$$

3 Gas-phase Molecules

To obtain the energy of the isolated molecule (gas-phase) we have placed each of them in the center of a large unit cell with 15 × 15.25 × 15.50 Å. Only the gamma point was used in the Brillouin zone integration, and the plane-wave cutoff energy has been fixed at 488.735 eV which is 12.25 % higher than the recommended value (`ENMAX`) for oxygen. The binding energy of each molecule is calculated as

$$\begin{aligned} E_b^{\mathrm{OH}} &= E_{tot}^{\mathrm{OH}} - E_{tot}^{\mathrm{H}} - E_{tot}^{\mathrm{O}} \\ E_b^{\mathrm{CO}} &= E_{tot}^{\mathrm{CO}} - E_{tot}^{\mathrm{C}} - E_{tot}^{\mathrm{O}} \ , \end{aligned} \tag{3}$$

and the results are shown in Table S2, which also presents bond lengths and comparison with previous results also obtained with DFT calculations with the PBE functional.[5]

Table S2 Binding energies (E_b) of the gas-phase molecules, and their relative deviation (ΔE_b) with respect to references values (E_b^{ref}).[5] Bond lengths $d^{\mathrm{H-O}}$ and $d^{\mathrm{C-O}}$ are also shown

Molecule	E_b (eV)	E_b^{ref} (eV)	ΔE_b (%)	$d^{\mathrm{H-O}}$ (Å)	$d^{\mathrm{C-O}}$ (Å)
OH	−4.75	−4.77	0.42	0.98	-
CO	−11.63	−11.66	0.26	-	1.14

4 Bulk Ag Properties

Before tackling the Ag(211) surface, we first performed convergence tests on bulk face-centered cubic (fcc) Ag and calculated its properties. The lattice parameter (a_0) was computed using different numbers of **k**-points for the Brillouin zone integration. The results are shown in Table S3, where it was found that a **k**-points mesh of $17 \times 17 \times 17$ was sufficient to achieve converged results for both a_0 and the total energy. The percentage difference in the lattice parameter is also given and is defined as $\Delta a_0 = \frac{(a_0^i - a_0^{largest})}{a_0^i} \times 100$, where a_0^i is the calculated lattice parameter and $a_0^{largest}$ is the most converged value. Similarly, ΔE_{tot} is defined as the difference between the total energy for a given calculation and the most converged one.

The convergence of the plane-wave cutoff energies (`ENCUT`) was also tested by computing a_0 with 1.00×, 1.25×, 1.50× , 1.75×, 200× , 2.25× and 2.50× the recommended value (`ENMAX`) for Ag, and the results are shown in Table S4. The obtained value of the lattice parameter of 4.07 Å agrees well with the experimental value of a_0 = 4.086 Å.[6]

Table S3 Convergence of the lattice parameter (a_0) and total energy (E_{tot}) determined by stress-tensor calculations of bulk primitive unit cell relaxation with variations of the k-points mesh ($n \times n \times n$).

n	**k**-points	a_0 (Å)	Δa_0 (%)	E_{tot} (eV)	ΔE_{tot} (meV)
4	10	4.086	0.393	−3.030 467 91	186
9	20	4.070	0.000	−3.234 923 02	−18
13	30	4.068	−0.049	−3.214 637 94	2
17	40	4.070	0.000	−3.212 069 65	4
21	50	4.071	0.024	−3.213 006 20	3
26	60	4.071	0.024	−3.217 727 64	−1
30	70	4.070	0.000	−3.216 443 95	0

Table S4 Convergence of the lattice parameter (a_0) and total energy (E_{tot}) determined by the stress-tensor calculation of bulk primitive unit cell relaxation with variations of the plane-wave cutoff energy with the k-mesh set as $17 \times 17 \times 17$.

`ENCUT` (eV)	a_0 (Å)	Δa_0 (%)	E_{tot} (eV)	ΔE_{tot} (meV)
249.884	4.030	−1.007	−3.205 804 29	6.27
312.355	4.064	−0.171	−3.218 765 90	−6.70
374.826	4.062	−0.221	−3.211 954 14	0.12
437.297	4.070	−0.024	−3.211 853 01	0.22
499.768	4.070	−0.024	−3.212 069 81	0.00
562.239	4.071	0.000	−3.212 197 57	−0.13
624.710	4.071	0.000	−3.212 290 45	−0.22

The density of states of bulk Ag is shown in Figure S1. As expected, the major contribution to the density of states come from the d band. The gravitational center (ε_d) of d-band is -4.4744 eV.

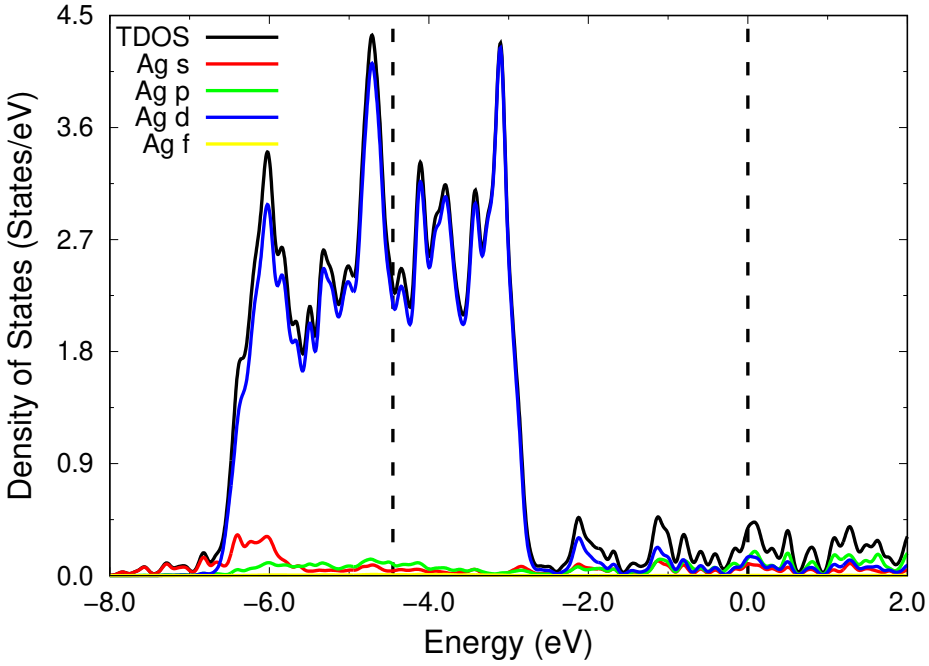

Figure S1 Local density of states (LDOS) for faced centered cubic bulk Ag. The Fermi energy is represented with a dashed vertical line at 0.00 eV **and the d-band center is represented with dashed line at** −4.45eV**.**

5 Stepped Ag(211) Clean Surface

The properties of the clean Ag(211) surface are reported here as a function of the **k**-mesh in order to determine a sufficiently converged set for posterior calculations. The slabs were built with a vacuum size of 16 Å, with 15 layers and (3×1) surface unit cell. The plane-wave cutoff energy has been fixed at `ENCUT` $= 281.074$ eV which is 12.25 % larger than the recommended value (`ENMAX`) for silver. The percentage of interlayer relaxation compared to the bulk structure was calculated for layers i and j as

$$\Delta d_{ij} = \frac{(d_{ij} - d_0) \times 100}{d_0}, \tag{4}$$

where d_{ij} is the spacing between layers i and j and d_0 is the separation between layers in the bulk.

The surface energy (σ) is calculated using the total energy of the slab (E_{slab}) with N layers, and the bulk total energy (E_{bulk}) as:

$$\sigma = \frac{1}{2}(\frac{E_{slab}}{3} - N \cdot E_{bulk}), \tag{5}$$

where E_{bulk} has been obtained as the slope of the slab energy as function of the number of layers. Note that the slab energy is divided by the number of atoms per layer (three).

The work function (φ) is calculated as the difference between the average electrostatic potential in the vacuum ($V_{elec}(\mathbf{r}_{vac})$) and the level Fermi energy, such as

$$\varphi = V_{elec}(\mathbf{r}_{vac}) - \epsilon_{\text{Fermi}}. \tag{6}$$

The results are shown in Figure S2 and Table S5, where it is seen that a **k**-mesh of $5 \times 4 \times 1$ provides sufficiently converged results for all three properties (one geometric, one energetic and one electronic property) and thus this mesh was used for all further calculations.

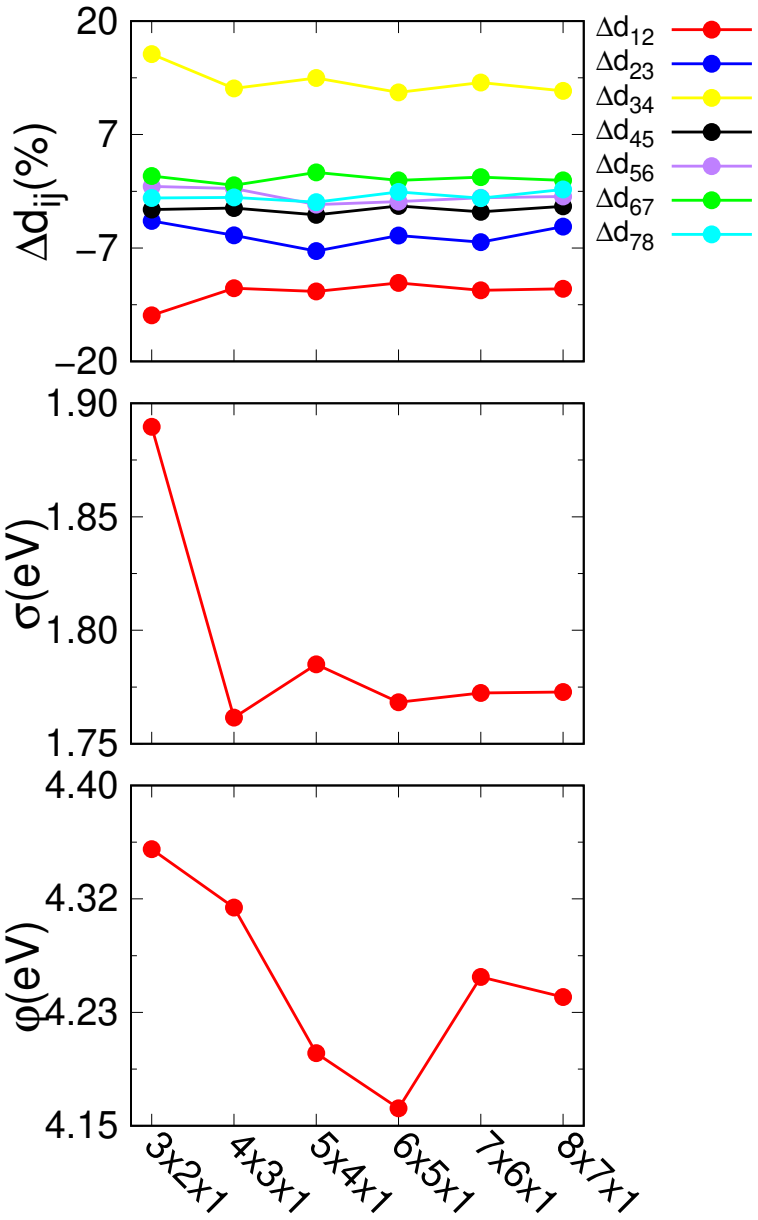

Figure S2 Interlayer relaxation, surface energy and work function as function of the k-mesh for Ag(211). The k-meshs $3 \times 2 \times 1$, $4 \times 3 \times 1$, $5 \times 4 \times 1$, $6 \times 5 \times 1$, $7 \times 6 \times 1$ **and** $8 \times 7 \times 1$ **have** 4, 6, 9, 12, 16 **and** 20 **k-points, respectively.**

Table S5 Convergence test for interlayer relaxation, surface energy and work function as a function of the k-mesh for Ag(211).

k-mesh	Δd_{12} (%)	Δd_{23} (%)	Δd_{34} (%)	Δd_{45} (%)	Δd_{56} (%)	Δd_{67} (%)	Δd_{78} (%)	σ (eV)	φ (eV)
$3 \times 2 \times 1$	−14.57	−3.47	16.11	−2.15	0.57	1.78	−0.79	1.89	4.35
$4 \times 3 \times 1$	−11.40	−5.19	12.09	−1.97	0.33	0.70	−0.72	1.77	4.31
$5 \times 4 \times 1$	−11.77	−7.03	13.31	−2.77	−1.57	2.21	−1.27	1.79	4.20
$6 \times 5 \times 1$	−10.76	−5.21	11.61	−1.71	−1.22	1.27	−0.08	1.77	4.16
$7 \times 6 \times 1$	−11.64	−5.98	12.77	−2.41	−0.76	1.65	−0.81	1.78	4.26
$8 \times 7 \times 1$	−11.47	−4.15	11.80	−1.77	−0.61	1.29	0.20	1.78	4.24

6 Substitution Doping Rh@Ag(211)

Before studying the interaction of the molecules with the doped surface, we have analysed how the presence of the dopant Rh atom redistributes the charges over the surface, which is given in Figure S3. It is seen that charge is transferred to the Rh atom from the Ag ones located in the subsurface.

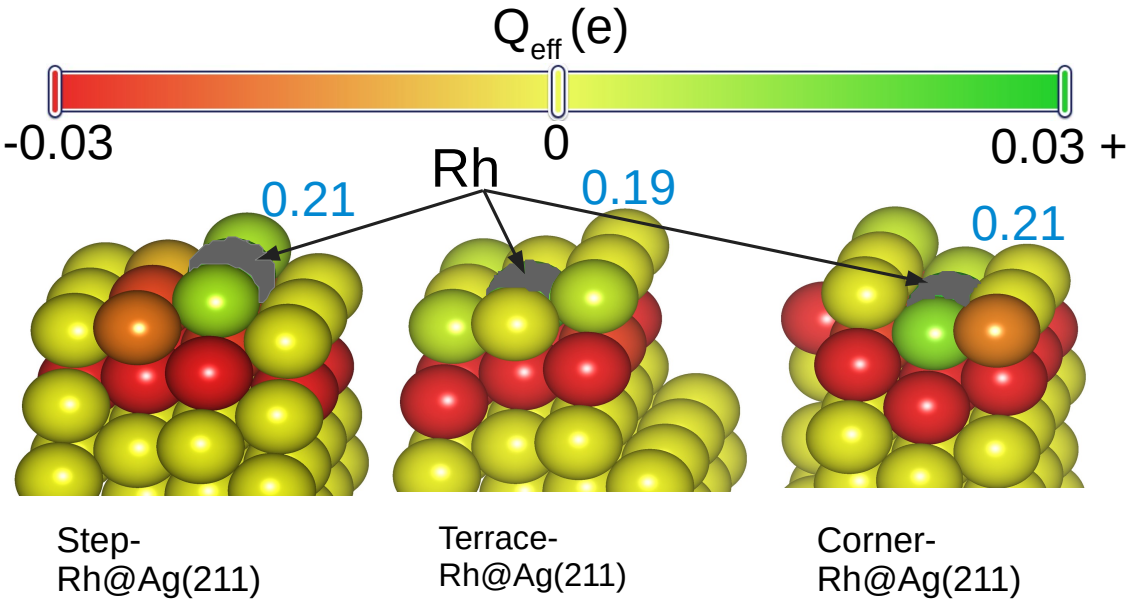

Figure S3 Bader charges for the Ag atoms in the doped surfaces. Q_{eff} **gradient bar refers to Ag atoms only, while the Rh charges are given in the numbers in blue.**

Also, it may be useful to analyze the effect of the dopant on the distance between the

nearest neighbors for each surface site, which is given in Table S6.

Table S6 Distance between the reference atom and its i^{th} nearest neighbor (d^i). The ECN values are also given for completeness.

Ref. Atom	d^1 (Å)	d^2 (Å)	d^3 (Å)	d^4 (Å)	d^5 (Å)	d^6 (Å)	d^7 (Å)	d^8 (Å)	d^9 (Å)	ECN (NNN)
Ag on Step	2.81	2.84	2.84	2.86	2.86	2.87	2.87	4.02	4.02	7.13
Ag on Terrace	2.84	2.84	2.86	2.86	2.87	2.87	2.90	2.90	2.92	8.97
Ag on Corner	2.81	2.84	2.84	2.88	2.88	2.90	2.91	2.91	2.94	9.90
Rh on Step	2.72	2.72	2.74	2.75	2.75	2.83	2.83	3.83	4.00	7.77
Rh on Terrace	2.75	2.75	2.79	2.80	2.80	2.81	2.81	2.85	2.85	9.59
Rh on Corner	2.79	2.80	2.80	2.80	2.82	2.82	2.84	2.84	2.87	10.52

7 Adsorption Properties

7.1 Adsorption Sites

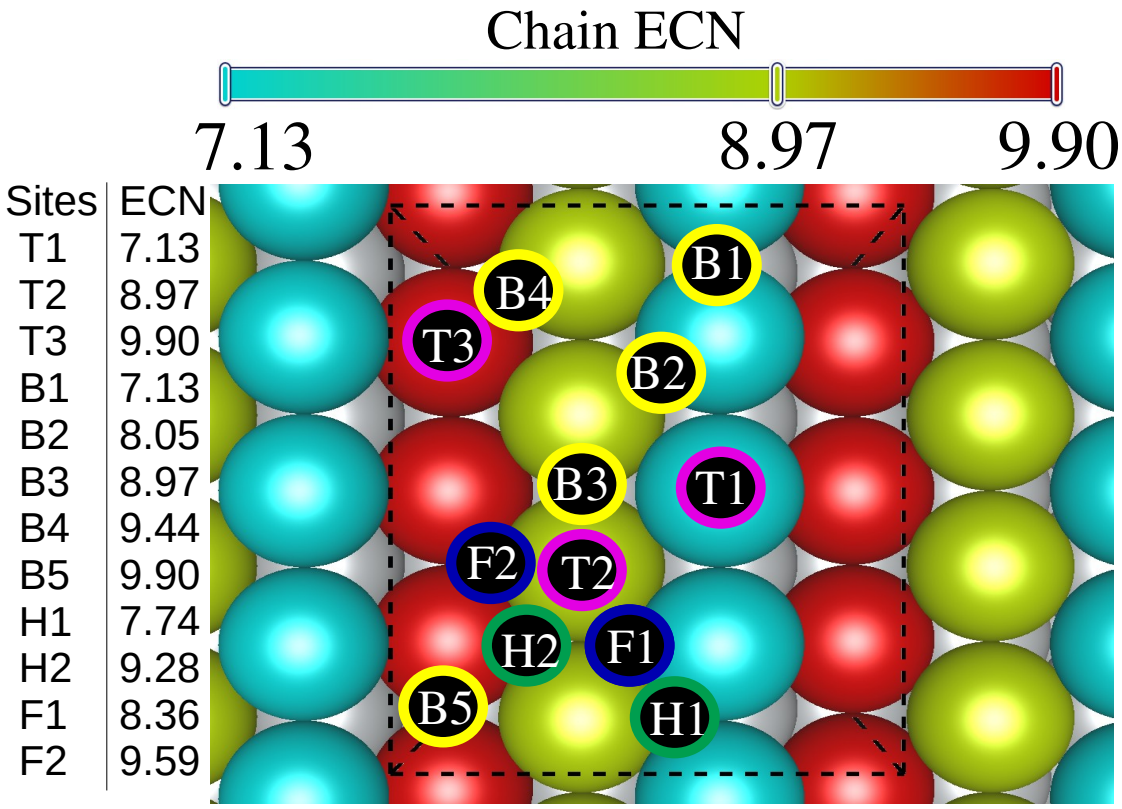

Figure S4 Ag(211)Top view with indication of Adsorptions sites top (T), Bridge (B) and Hollow (H). A color scale is assigned to surface atoms according to the ECN. The exact values for each Site are indicated in the table on the left.

We have performed calculations for the two molecules (OH and CO) adsorbed on the Ag(211) slab described above. For all adsorption calculations we have used the 5x4x1 **k**-mesh and an energy cutoff of 488.735 eV, which is 12.25 % higher than the largest recommended value (the `ENMAX` of oxygen given in Table S1).

A schematic representation of the adsorption sites considered here is shown in Figure S4. In total, there are three top sites (T1, T2 and T3), five bridge sites (B1, B2, B3, B4 and B5), two hcp hollow sites (H1 and H2) and two fcc hollow sites (F1 and F2). Note that, as there are no atoms on bridge and hollow sites, they do not have an actual coordination

number. In this figure we provide estimated ECN values for such sites as an average of the ECN of the atoms that define them. For example, the ECN of the B2 site is the average ECN of the atoms at T1 and T2.

The adsoption energy (E_{ad}) is calculated from the total energy of the clean surface (E_{tot}^{surf}), that of the gas-phase molecule (E_{tot}^{mol}) and the total energy of the adsorbed configuration ($E_{tot}^{mol/surf}$) as

$$E_{ad} = E_{tot}^{mol/surf} - E_{tot}^{surf} - E_{tot}^{mol} \ . \tag{7}$$

For this reason the energy of the gas-phase molecule is presented in the next section.

7.2 Adsorption of OH on Ag(211)

In Table S7 we provide the numerical values for the adsorption energy, the distance between the molecule and the closest atom on the surface ($d^{\mathrm{O-Ag}}$), as well as the OH bond distance ($d^{\mathrm{O-H}}$) and angle of the molecule (α_{HOTM}) for all adsorption sites.

Table S7 Adsorption energy (E_{ad}), work function (φ) and geometric parameters ($d^{\mathrm{O-H}}$, $d^{\mathrm{O-Ag}}$ and α_{HOTM}) for each adsorption site for OH **on Ag(211).**

Site	E_{ad} (eV)	φ (eV)	$d^{\mathrm{O-Ag}}$ (Å)	$d^{\mathrm{O-H}}$ (Å)	α_{HOTM} (°)
B1	−2.70	4.27	2.16	0.97	58.55
B3	−2.51	4.25	2.26	0.97	58.66
B5	−2.76	4.12	2.31	0.98	58.55
T1	−1.90	4.54	2.03	0.97	58.73
T3	−2.45	4.19	2.18	0.97	58.71
F1	−2.68	4.09	2.30	0.97	58.22
H1	−2.75	4.13	2.25	0.97	58.28
H2	−2.50	4.10	2.28	0.97	58.15

7.3 Adsorption of CO on Ag(211)

In Table S8 we provide the numerical values for the adsorption energy, work function, the distance between the molecule and the closest atom on the surface ($d^{\mathrm{C-Ag}}$), as well as

the CO bond distance (d^{C-O}) and angle of the molecule (α_{OCTM}) for all adsorption sites.

Table S8 Adsorption energy (E_{ad}), work function (φ) and geometric parameters (d^{C-O}, d^{C-Ag} and α_{OCTM}) for CO on Ag(211) on each adsorption site.

Site	E_{ad} (eV)	φ (eV)	d^{O-Ag} (Å)	d^{O-H} (Å)	α_{OCTM} (°)
B1	−0.48	4.37	2.24	1.16	58.32
B3	−0.38	4.32	2.29	1.16	58.20
T1	−0.51	4.19	2.13	1.15	58.09
T2	−0.42	4.18	2.13	1.15	58.15
T3	−0.33	4.30	2.24	1.16	58.97

7.4 Adsorption of OH on Rh@Ag(211)

The values for the adsorption energy, the work function, the distance between the molecule and the dopant (d^{O-Rh}), the distance between the molecule and the closest Ag atom at surface (d^{O-Ag}), the bond length of the molecule (d^{O-H}) and the angle of the molecule with the surface (α_{HOTM}) are given for all adsorption sites in Figure S9.

Table S9 Adsorption energy (E_{ad}), work function (φ) and geometrical parameters for OH on Rh doped Ag(211) on each adsorption site.

Site	Rh Site	E_{ad} (eV)	φ (eV)	d^{Rh-O} (Å)	d^{Ag-O} (Å)	d^{O-H} (Å)	α_{HOTM} (°)
B1	Step	−3.26	4.50	2.00	2.32	0.98	48.13
B1	Terrace	−2.75	4.22	4.97	2.26	0.98	58.05
B3	Terrace	−2.78	4.24	2.04	2.44	0.98	58.38
T1	Step	−3.10	4.56	1.92	3.37	0.98	48.36
T3	Corner	−2.71	4.23	2.07	2.21	0.98	58.40
F1	Terrace	−2.74	4.13	2.07	2.40	0.97	58.16
F1	Corner	−2.69	4.15	4.06	2.26	0.97	58.68
H1	Terrace	−2.75	4.14	2.08	2.39	0.97	58.03
H1	Corner	−2.74	4.17	4.84	2.27	0.97	58.90
H2	Corner	−2.57	4.12	2.11	2.34	0.97	58.12

7.5 Adsorption of CO on Rh@Ag(211)

The values for the adsorption energy, work function, distance between the molecule and the dopant (d^{C-Rh}), distance between the molecule and the closest Ag atom at surface

(d^{C-Ag}), the bond length of the molecule (d^{C-O}), and the angle of the molecule with the surface (α_{OCTM}) are given for all adsorption sites.

Table S10 Adsorption energy (E_{ad}), work function (φ) and geometric parameters for CO on Rh doped Ag(211).

Site	Rh Site	E_{ad} (eV)	φ (eV)	d^{Rh-C} (Å)	d^{Ag-C} (Å)	d^{C-O} (Å)	α_{OCTM} (°)
B1	Terrace	−0.37	4.36	3.64	2.26	1.15	58.24
B1	Corner	−0.46	4.38	6.01	2.21	1.16	58.71
T1	Step	−2.43	4.75	1.83	3.27	1.17	58.02
T1	Terrace	−0.49	4.24	4.28	2.12	1.15	58.06
T1	Corner	−0.49	4.17	6.02	2.09	1.15	58.59
T2	Step	−0.34	4.75	3.59	2.16	1.14	58.06
T2	Terrace	−2.38	4.49	1.84	3.23	1.17	58.00
T2	Corner	−0.32	4.21	4.03	2.15	1.15	58.50
T3	Corner	−2.03	4.39	1.84	2.89	1.17	57.87
F1	Corner	−0.37	4.37	4.14	2.24	1.17	58.52

7.6 Gibbs Free Energies of Adsorption

The Gibbs free energies of adsorption (G_{ad}) were calculated for the lowest energy structures at room temperature as:

$$G_{ad} = G_{tot}^{mol/surf} - G_{tot}^{surf} - G_{tot}^{mol} \ . \tag{8}$$

Each term in this equations was calculated with the DFT total energy E_{tot}, and including zero point energy (ZPE), enthalpic and entropic contributions as:

$$G = E_{tot} + ZPE + \int C_p dT - TS. \tag{9}$$

To calculate such contributions, we have first computed DFT vibrational frequencies for the gas-phase molecule and for the adsorbed configuration with the atomic positions of the substrate fixed. Such values were then used in standard statistical mechanics expressions to calculate the properties at the harmonic limit, using the atomic simulation environment package[7]. The fugacity in CO calculation is 5562 Pa.

It is known that the PBE functional provides inconsistent thermochemical values for gas-phase CO, and for this reason we have added a gas-phase correction (GPC) of -0.51eV to its energy as calculated in the literature[8]. The lowest energy structure for the CO adsorption on both doped and non-doped substrates (T1-CO/Ag(211) and T1-Step-CO/Rh@Ag(211)) were selected, and Table S11 gather the results.

Table S11 Calculated energy contributions for the Gibbs free energy for the gas-phase molecule and adsorbed configurations on the lowest energy site of the substrates.

System	E_{tot} (eV)	ZPE (eV)	$\int CpdT$ (Å)	$-TS$ (eV)	GPC (eV)	G (eV)
CO	-14.91	0.132	0.065	-0.681	-0.51	-15.90
CO/Ag(211)	-148.88	0.164	0.071	-0.152	-	-148.80
CO/Rh@Ag(211)	-154.05	0.201	0.021	-0.162	-	-153.93

As the atomic position of the atoms in the slab were considered fixed in the vibrational calculations, $G_{tot}^{surf} = E_{tot}^{surf}$. Therefore, taking into account the values on Table S11, we obtain $G_{ad} = 0.56$eV for T1- CO/Ag(211) and $G_{ad} = -1.33$eV for T1-step CO/Rh@Ag(211).

7.7 Adsorption Barrier

To check for the possibility of an adsorption barrier, we have performed calculations starting at the optimized adsorbed configuration and increasing the height of the C atom while relaxing the height of the oxygen one. The substrate atoms were kept frozen during the whole process. As can be seen in Figure S5, our calculations predict that there is no energy barrier for the adsorption of CO on doped or non-doped substrates

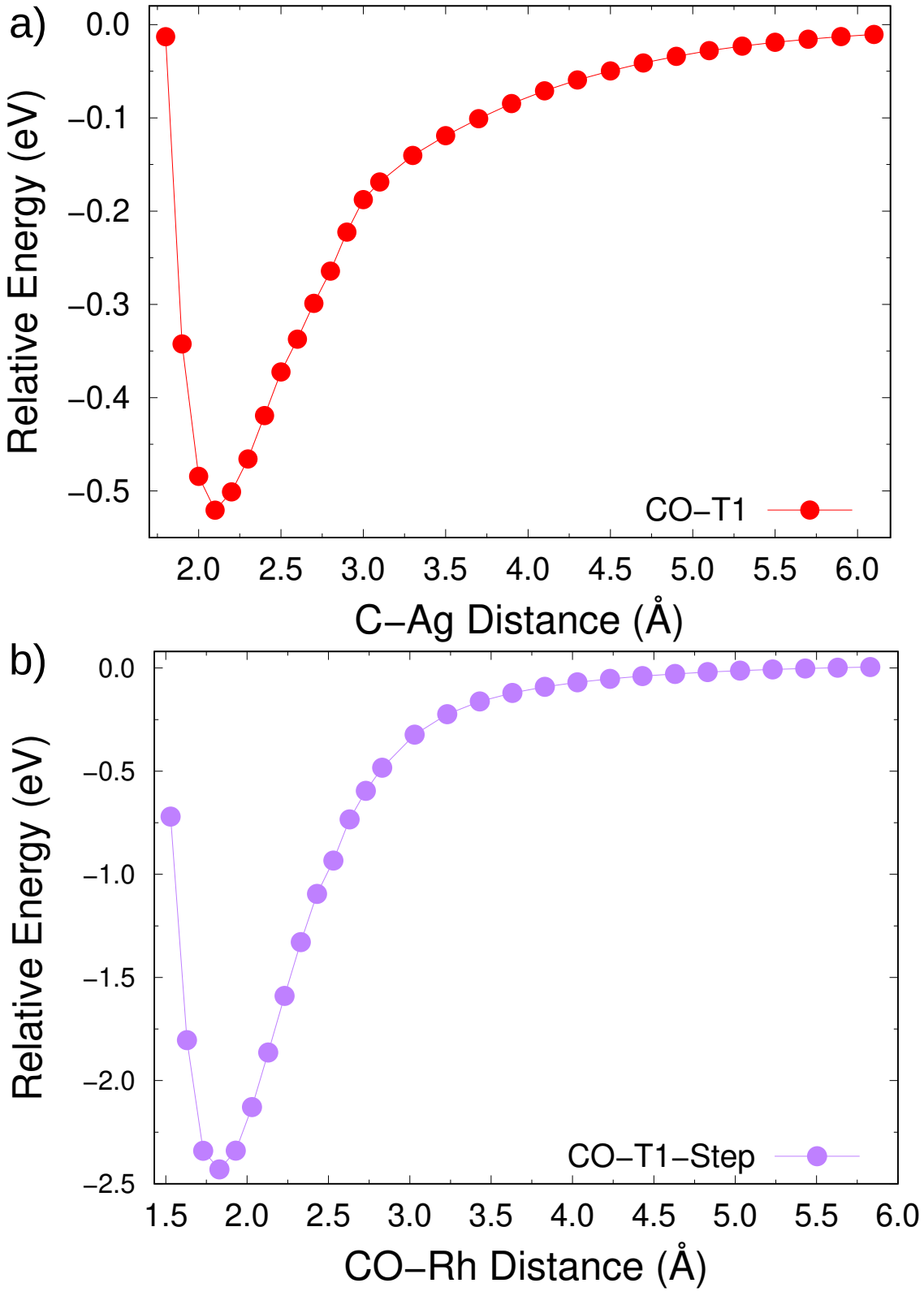

Figure S5 Relative energy as a function of the C-TM distance for structures a) CO/T1 for non-doped substrate and b) CO/T1-Rh@Ag(211)-Step.

7.8 Adsorption on nanoclusters and benchmarking

In this section, we assess if the conclusions of our work would be maintained if a higher level DFT functional was used. We also take the opportunity to check the effect of using a nanocluster instead of a stepped surface.

As a prototypical silver cluster, we have chosen the Ag_8 structure reported in the literature.[9] Calculations on the CO adsorption on both Ag_8 and Ag_7Rh were performed using the GAMESS package,[10] with the ωB97XD[11] and PBE[5] functionals. The SBKJC basis set[12,13] including an effective core potential was employed.

The results are gathered in Fig. S6. First of all, it is clear that both ωB97XD and PBE+D3 approaches correctly predicts that the presence of the single Rh dopant largely enhances the adsorption energy on the nanoclusters, just as was concluded for the (211) surfaces with the PBE results in the manuscript. The PBE+D3 approach predicts an adsorption energy 0.3eV higher than the ωB97XD results, which is within the expected accuracy of DFT calculations.

It was shown in the manuscript that the adsorption energies are predicted to be higher when the molecule binds to surface atoms with low coordination numbers. Therefore, one could expect that adsorption on the small cluster would yield a higher magnitude of E_{ad}, which is what can be observed by comparing the surfaces with the clusters in Fig. S6. Still, the trend of chemisorption when the dopant is added continues to be observed in clusters as a substrate. While for non-doped structure, the probe continues to be adsorbed as physisorption.

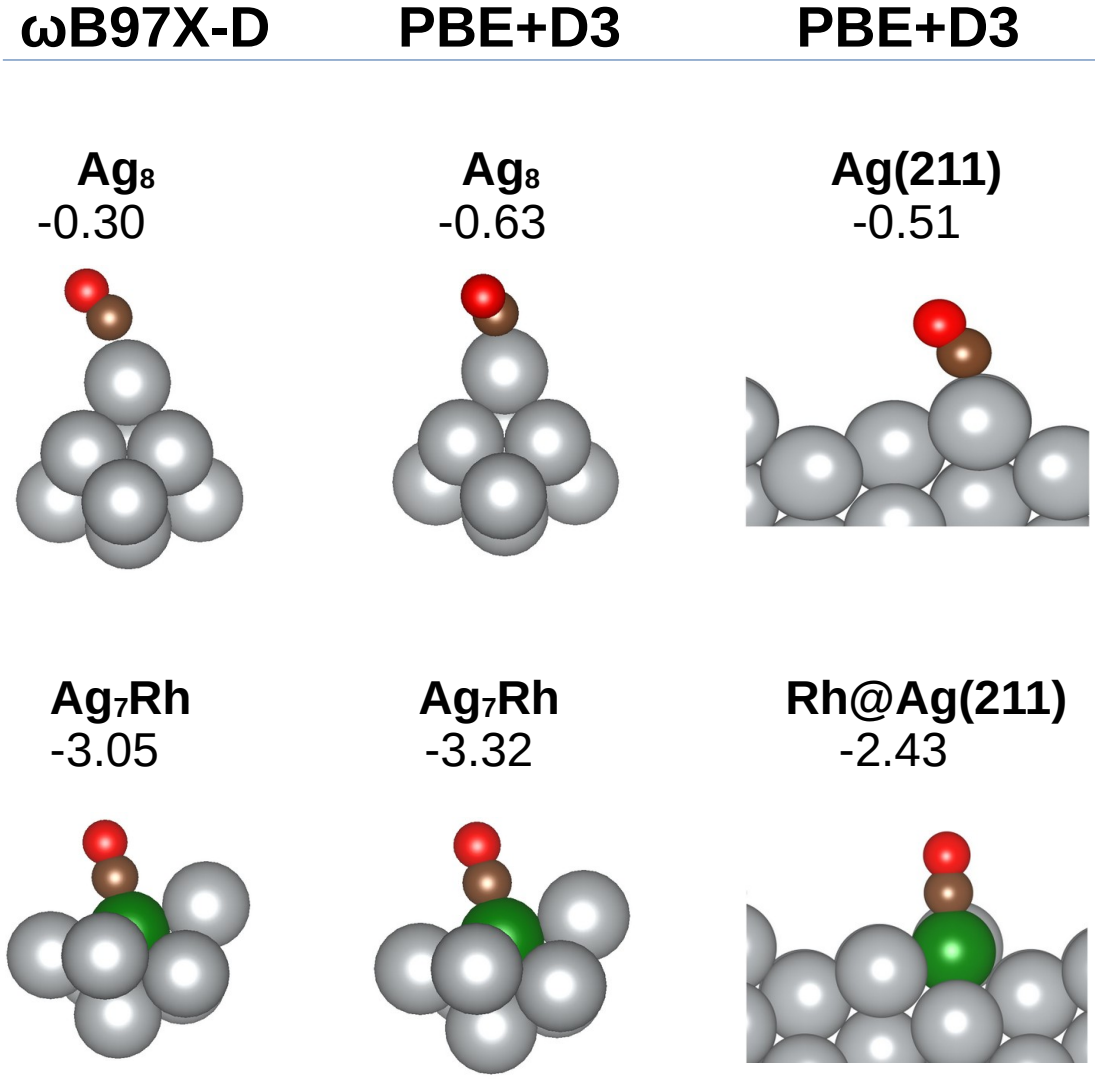

Figure S6 Adsorption of CO on doped and non doped surfaces substrates, with adsorption energies given in eV. Clusters were calculated in GAMESS while the surfaces were calculated with VASP.

References

1 Kresse, G.; Furthmüller, J. Efficient Iterative Schemes for *Ab initio* Total-energy Calculations Using a Plane-wave Basis set. *Phys. Rev. B* **1996**, *54*, 11169–11186, DOI: 10.1103/physrevb.54.11169.

2 Kresse, G.; Joubert, D. From Ultrasoft Pseudopotentials to the Projector Augmented-wave Method. *Phys. Rev. B* **1999**, *59*, 1758–1775, DOI: 10.1103/physrevb.59.1758.

3 Hoppe, R. Effective Coordination Numbers (ECoN) and Mean Active Fictive Ionic Radii (MEFIR). *Z. Kristallogr.* **1979**, *150*, 23–52, DOI: 10.1524/zkri.1979.150.1-4.23.

4 Da Silva, J. L. F. Effective Coordination Concept Applied for Phase Change $(GeTe)_m(Sb_2Te_3)_n$ Compounds. *J. Appl. Phys.* **2011**, *109*, 023502, DOI: 10.1063/1.3533422.

5 Perdew, J. P.; Burke, K.; Ernzerhof, M. Generalized Gradient Approximation Made Simple. *Phys. Rev. Lett.* **1996**, *77*, 3865–3868, DOI: 10.1103/physrevlett.77.3865.

6 Haynes, W. M. *CRC Handbook of Chemistry and Physics*; CRC press, 2014.

7 Larsen, A. H.; Mortensen, J. J.; Blomqvist, J.; Castelli, I. E.; Christensen, R.; Dułak, M.; Friis, J.; Groves, M. N.; Hammer, B.; Hargus, C., et al. The atomic simulation environment—a Python library for working with atoms. *J. Condens. Matter Phys.* **2017**, *29*, 273002, DOI: 10.1088/1361-648X/aa680e.

8 Peterson, A. A.; Abild-Pedersen, F.; Studt, F.; Rossmeisl, J.; Nørskov, J. K. How copper catalyzes the electroreduction of carbon dioxide into hydrocarbon fuels. *Energy Environ. Sci* **2010**, *3*, 1311–1315, DOI: 10.1039/C0EE00071J.

9 Heiles, S.; Logsdail, A. J.; Schäfer, R.; Johnston, R. L. Dopant-induced 2D–3D transition in small Au-containing clusters: DFT-global optimisation of 8-atom Au–Ag nanoalloys. *Nanoscale* **2012**, *4*, 1109–1115, DOI: 10.1039/C1NR11053E.

10 Schmidt, M. W.; Baldridge, K. K.; Boatz, J. A.; Elbert, S. T.; Gordon, M. S.; Jensen, J. H.; Koseki, S.; Matsunaga, N.; Nguyen, K. A.; Su, S., et al. General atomic and molecular electronic structure system. *J. Comput. Chem.* **1993**, *14*, 1347–1363, DOI: 10.1002/jcc.540141112.

11 Chai, J.-D.; Head-Gordon, M. Long-range corrected hybrid density functionals with damped atom–atom dispersion corrections†. *Phys. Chem.* **2008**, *10*, 6615–6620, DOI: 10.1039/B810189B.

12 Stevens, W. J.; Basch, H.; Krauss, M. Compact effective potentials and efficient shared-exponent basis sets for the first-and second-row atoms. *Chem. Phys* **1984**, *81*, 6026–6033, DOI: 10.1063/1.447604.

13 Stevens, W. J.; Krauss, M.; Basch, H.; Jasien, P. G. Relativistic compact effective potentials and efficient, shared-exponent basis sets for the third-, fourth-, and fifth-row atoms. *Can. J. Chem.* **1992**, *70*, 612–630, DOI: 10.1139/v92-085.